

Understanding the evolution of Atira-class asteroid 2019 AQ₃, a major step towards the future discovery of the Vatira population

C. de la Fuente Marcos¹^{*} and R. de la Fuente Marcos²

¹ Universidad Complutense de Madrid, Ciudad Universitaria, E-28040 Madrid, Spain

² AEGORA Research Group, Facultad de Ciencias Matemáticas, Universidad Complutense de Madrid, Ciudad Universitaria, E-28040 Madrid, Spain

Accepted 2019 May 21. Received 2019 May 20; in original form 2019 January 10

ABSTRACT

Orbiting the Sun at an average distance of 0.59 au and with the shortest aphelion of any known minor body, at 0.77 au, the Atira-class asteroid 2019 AQ₃ may be an orbital outlier or perhaps an early indication of the presence of a new population of objects: those following orbits entirely encompassed within that of Venus, the so-called Vativas. Here, we explore the orbital evolution of 2019 AQ₃ within the context of the known Atiras to show that, like many of them, it displays a present-day conspicuous coupled oscillation of the values of eccentricity and inclination, but no libration of the value of the argument of perihelion with respect to the invariable plane of the Solar system. The observed dynamics is consistent with being the result of the combined action of two dominant perturbers, the Earth–Moon system and Jupiter, and a secondary one, Venus. Such a multiperturber-induced secular dynamics translates into a chaotic evolution that can eventually lead to a resonant behaviour of the Lidov–Kozai type. Asteroid 2019 AQ₃ may have experienced brief stints as a Vatira in the relatively recent past and it may become a true Vatira in the future, outlining possible dynamical pathways that may transform Atiras into Vativas and vice versa. Our results strongly suggest that 2019 AQ₃ is only the tip of the iceberg: a likely numerous population of similar bodies may remain hidden in plain sight, permanently confined inside the Sun’s glare.

Key words: methods: numerical – methods: statistical – celestial mechanics – minor planets, asteroids: general – minor planets, asteroids: individual: 2019 AQ₃ – planets and satellites: individual: Venus.

1 INTRODUCTION

The innermost section of the Solar system, that within Venus’ orbit, is still far from well studied as it mostly remains confined inside the Sun’s glare as seen from the Earth. So far, no minor bodies have ever been observed to orbit the Sun entirely within Venus’ path, but they are assumed to exist: the so-called Vativas (Greenstreet, Ngo & Gladman 2012). Bordering the hypothetical Vatira orbital realm (aphelion distance, Q , in the range 0.307–0.718 au) there is only one known Atira, 2019 AQ₃ with $Q = 0.77$ au.

Atira-class asteroids —also known in the literature as Apoheles (Tholen 1998),¹ or Inner-Earth objects, IEOs (Michel et al. 2000; Zavadny et al. 2008)— have $0.718 \text{ au} < Q < 0.983 \text{ au}$ (Greenstreet et al. 2012). As of 2019 May 20, there are only 19 known Atiras because, like Venus or Mercury, they can only be observed near their maximum elongation (east or west; see e.g. Masi 2003), when their angular separation from the Sun is greatest —in the interval (18°, 28°) for Mercury and (45°, 47°) for

Venus. The relevance and implications of studying minor bodies at small solar elongations was first discussed by Tholen & Whiteley (1998) and Whiteley & Tholen (1998), and the origin of those known remains an open question (Greenstreet, Ngo & Gladman 2010). Although a long-term stable asteroid belt located at 0.09–0.21 au from the Sun has been predicted (Evans & Tabachnik 1999, 2002), no positive detections have been reported yet (Durda et al. 2000; Schumacher & Gay 2001; Steffl et al. 2013). It is however unclear whether other processes may remove material from this region (see e.g. Farinella et al. 1994; Stern & Durda 2000; Vokrouhlický, Farinella & Bottke 2000; Warell, Karlsson & Skoglöv 2003).

Atira-class asteroids can experience close encounters with Mercury, Venus, and the Earth–Moon system, but de la Fuente Marcos & de la Fuente Marcos (2018) have shown that many known Atiras display a conspicuous behaviour that somehow resembles the one induced by the Lidov–Kozai mechanism (Kozai 1962; Lidov 1962); such a circumstance opens the door to a chaotic but relatively stable dynamical scenario. This interpretation is consistent with the one presented by Ribeiro et al. (2016), where it is argued that many Atiras remain on regular orbits for at least 1 Myr. Here, we investigate the dynamical evolution

^{*} E-mail: nbplanet@ucm.es

¹ <http://defendgaia.org/bobk/ccc/cc070998.html>

of 2019 AQ₃, a recently discovered near-Earth asteroid (NEA) that has the shortest aphelion of any known minor body, 0.77 au. This paper is organized as follows. In Section 2, we present the available data on this object and the tools used in our study. The orbital evolution of 2019 AQ₃ is explored in Section 3. Our results are discussed in Section 4 and our conclusions are summarized in Section 5.

2 DATA AND METHODS

The source of most of the data used in this research is Jet Propulsion Laboratory’s Solar System Dynamics Group Small-Body Database (JPL’s SSDG SBDB, [Giorgini, Chodas & Yeomans 2001](#); [Giorgini 2011, 2015](#))² and JPL’s HORIZONS³ ephemeris system ([Giorgini et al. 1996](#); [Standish 1998](#); [Giorgini & Yeomans 1999](#)). This includes orbit determinations, covariance matrices, initial conditions (positions and velocities in the barycentre of the Solar system) for planets and minor bodies referred to epoch JD 2458600.5 (2019-Apr-27.0) TDB (Barycentric Dynamical Time) —which is the zero instant of time in the figures, J2000.0 ecliptic and equinox— ephemerides, and other input data. When quoted, statistical parameters have been computed in the usual way (see e.g. [Wall & Jenkins 2012](#)).

2.1 Atira-class asteroid 2019 AQ₃: the data

Asteroid 2019 AQ₃ was discovered on 2019 January 4 ([Buzzi et al. 2019](#)) by the Zwicky Transient Facility observing system ([Smith et al. 2014](#); [Bellm & Kulkarni 2017](#)) at Palomar Mountain. The Pan-STARRS project ([Kaiser 2004](#); [Kaiser et al. 2004](#)) team found precovery images acquired in 2015 ([Chambers et al. 2019](#)). With both old and new data, the orbit determination of 2019 AQ₃ shown in Table 1 was computed on 2019 February 3 and it is based on 49 observations for a data-arc span of 1199 d.

Asteroid 2019 AQ₃ is relatively large with an absolute magnitude of 17.6 mag (assumed $G = 0.15$), which suggests a diameter in the range 0.52–4.00 km for an assumed albedo in the range 0.60–0.01. It is a member of the Atira dynamical class (see above), but also an NEA because its perihelion distance is under 1.3 au. Its aphelion distance, 0.77 au, is the shortest of any known minor body —followed by (418265) 2008 EA₃₂ at 0.80 au. It has the shortest sidereal orbital period of any known Atira and the second shortest of any known minor body with nearly 165 d; Aten-class ($a < 1$ au and $Q > 0.983$ au) asteroid 2016 XK₂₄ has the shortest, with slightly over 161 d, but its orbit determination is very uncertain as it is based on seven observations for a data-arc span of 1 d. Within the Atira group, 2019 AQ₃ has the highest value of the orbital inclination, 47°.2. It is probably the third largest member of the group, together with 2018 JB₃; the synchronous binary asteroid (163693) Atira ([Rivera-Valentin et al. 2017](#)) is the largest with 4.8 km, followed by 418265.

2.2 N -body simulations

In order to explore the orbital evolution of 2019 AQ₃, we have performed full N -body simulations using a soft-

Table 1. Values of the Heliocentric Keplerian orbital elements of 2019 AQ₃ and their associated 1σ uncertainties. The orbit determination is referred to epoch JD 2458600.5 (2019-Apr-27.0) TDB (J2000.0 ecliptic and equinox). Source: JPL’s SBDB.

Orbital parameter	Value $\pm 1\sigma$ uncertainty
Semimajor axis, a (au)	= 0.58866153 \pm 0.00000008
Eccentricity, e	= 0.3143098 \pm 0.0000005
Inclination, i (°)	= 47.2186 \pm 0.0009
Longitude of the ascending node, Ω (°)	= 64.4873 \pm 0.0004
Argument of perihelion, ω (°)	= 163.1518 \pm 0.0005
Mean anomaly, M (°)	= 118.4994 \pm 0.0009
Perihelion, q (au)	= 0.4036395 \pm 0.0000003
Aphelion, Q (au)	= 0.77368361 \pm 0.00000010
Absolute magnitude, H (mag)	= 17.6 \pm 0.5

ware⁴ that implements a fourth-order version of the Hermite integration scheme ([Makino 1991](#); [Aarseth 2003](#)). We have carried out calculations under the Newtonian approximation as described by [de la Fuente Marcos & de la Fuente Marcos \(2012\)](#), but also under the post-Newtonian approximation as in [de la Fuente Marcos, de la Fuente Marcos & Aarseth \(2015\)](#) because the perihelion distance of 2019 AQ₃ becomes comparable (see Section 3.5) to those of the so-called relativistic asteroids (see table 2 in [Benitez & Gallardo 2008](#)). The impact of the uncertainties of the orbit determination on our results has been evaluated using the covariance matrix methodology described in [de la Fuente Marcos & de la Fuente Marcos \(2015a\)](#).

The integrator used in this work is not symplectic; therefore, it can be argued that the accumulation of errors during long calculations could be important and, since the trajectory of 2019 AQ₃ and those of other Atiras studied here are chaotic, this may lead to significant changes in the long-term evolution of these objects as portrayed by our simulations. The issue of symplectic integration versus other approaches, such as the fourth-order version of the Hermite integration scheme ([Makino 1991](#)) used here or time-symmetric versions of these algorithms, has been discussed in detail by e.g. [Hernandez & Bertschinger \(2015, 2018\)](#) and it is outside the scope of this work. It is however worth to mention that [de la Fuente Marcos & de la Fuente Marcos \(2012\)](#) show explicitly (see their fig. 3) that results from the integration scheme used here are consistent with those obtained using other techniques, e.g. [Varadi, Runnegar & Ghil \(2003\)](#) or [Laskar et al. \(2011\)](#).

3 ORBITAL EVOLUTION

The analysis in [de la Fuente Marcos & de la Fuente Marcos \(2018\)](#) pointed out that many Atiras have arguments of perihelion, ω , in the neighbourhood of 0° or 180°, which means that the nodal points —where the orbit crosses the ecliptic— are located at perihelion and at aphelion ([Milani et al. 1989](#)). However, this could be due to observational bias (see e.g. [Ribeiro et al. 2016](#)) as the Atiras are preferentially discovered near aphelion.

For 2019 AQ₃, $\omega = 163^\circ.2$ and given the fact that $Q = 0.77$ au (the semimajor axis of Venus is 0.72 au with a nearly circular orbit) the direct perturbation of Venus might be significant. On the other hand, [de la Fuente Marcos & de la Fuente Marcos \(2018\)](#)

² <https://ssd.jpl.nasa.gov/sbdb.cgi>

³ <https://ssd.jpl.nasa.gov/?horizons>

⁴ <http://www.ast.cam.ac.uk/~sverre/web/pages/nbody.htm>

also discussed an eccentricity–inclination ($e - i$) inverse relationship that is ubiquitous within the Atira group; this property is also present in the case of 2019 AQ₃, relatively low eccentricity (0.31) but high inclination (47:2), see Table 1. These facts suggest that the Lidov–Kozai mechanism might control the orbital evolution of these objects; the Lidov–Kozai resonance, within the context of NEAs, has been studied by e.g. Michel & Thomas (1996) and de la Fuente Marcos & de la Fuente Marcos (2015b). The Lidov–Kozai mechanism in the context of multiplanet systems has been studied by Libert & Tsiganis (2009). However, the Lidov–Kozai mechanism requires the concurrent oscillation of the values of three orbital parameters (in the frame of reference of the invariable plane of the studied system): e , i , and ω . Direct N -body simulations should be able to either confirm or reject the presence of a simultaneous, repetitive variation of the values of e , i , and ω throughout the orbital evolution of the Atiras.

3.1 Short-term evolution

Figure 1, left-hand side set of panels, shows the short-term evolution (from 1 Myr into the past to 1 Myr into the future) of the values of a number of relevant parameters for the nominal orbit of 2019 AQ₃. Close encounters with the Earth–Moon system are not possible, but both the top and second to top panels in Fig. 1 show that the peculiar dynamics of 2019 AQ₃ leads to avoiding close encounters with both Venus and Mercury for the most part; only a few flybys within the Hill radius of Venus, 0.0067 au, are recorded in our calculations. The third to top panel shows the evolution of the value of the so-called Lidov–Kozai parameter, $\sqrt{1 - e^2} \cos i$ that oscillates significantly during most of the displayed time interval. Michel & Thomas (1996) and de la Fuente Marcos & de la Fuente Marcos (2015b) have shown that the value of the Lidov–Kozai parameter of NEAs tends to change only slightly when the Lidov–Kozai resonance is in effect (see also Section 3.3.1).

The value of the semimajor axis (fourth to top panel) changes by about 5 per cent during the time interval displayed, drifting from one quasi-constant value to a relatively close one (also quasi-constant) for most of the integrated time. The evolution is chaotic as orbits starting arbitrarily close to each other diverge relatively quickly (not shown in the figures), but the overall dynamics resembles that of stable chaotic orbits (see e.g. Milani & Nobili 1992). On the other hand, the values of e (fourth to bottom panel) and i (third to bottom panel) oscillate, alternating high e and i . It is clear that, although the evolution somehow resembles the one found in the Lidov–Kozai scenario for e and i (Kozai 1962; Lidov 1962), the overall dynamical situation is different as the value of ω (second to bottom panel) circulates. The lack of libration in ω confirms that this object is not currently subjected to a Lidov–Kozai resonance (but see Section 3.2 for a proper analysis in the frame of reference of the invariable plane of the system).

The nodal distances from the Sun (bottom panel) show the location of the points where the orbit crosses the ecliptic; encounters with planetary bodies may take place there. An oscillation is observed, but the current layout ($t = 0$) shows the descending node located between Mercury’s perihelion and aphelion, and the ascending one beyond Venus. This explains well why the distances from Mercury and Venus remain large enough to avoid close flybys; the dynamical context that controls the orbital evolution of 2019 AQ₃ is protecting it from approaching the innermost planets too closely. A similar behaviour has been

previously observed in the case of Venus co-orbitals (see e.g. de la Fuente Marcos & de la Fuente Marcos 2012, 2013a, 2014).

On the other hand, asteroid 2019 AQ₃ is not currently in mean-motion resonance with any planet; it is, however, in near-mean-motion resonance with Mercury (15:8), Venus (11:15), the Earth (9:20), Mars (6:25), and Jupiter (1:26) —the ones with Mars, Mercury, and Jupiter (in this order) are the closest. In Section 3.4, we show that the Earth–Moon system and Jupiter are the main secular perturbers of 2019 AQ₃.

Figure 2 shows the short-term evolution of e , i , and ω of 2019 AQ₃ (red triangles) within the context of those of other Atiras —(418265) 2008 EA₃₂ (gold squares), 2010 XB₁₁ (blue circles), and 2018 JB₃ (black diamonds)— also displaying the behaviour pointed out above (see also fig. 1 in de la Fuente Marcos & de la Fuente Marcos 2018). It cannot be discarded that a sizeable population of stable (in the sense of remaining confined within a relatively small section of the orbital parameter space) Atiras/Vatiras may share high values of the inclination, particularly if their arguments of perihelia are close to 90° or 270° so they avoid close encounters with Venus at aphelion.

If the known Atiras are not subjected to a present-day Lidov–Kozai resonance, they should exhibit obvious differences when compared with other NEAs truly engaged in Lidov–Kozai resonant behaviour. Figure 3 shows the evolution of the relevant parameters of representative minor bodies. NEAs 2012 FC₇₁ (purple squares in Fig. 3, left-hand side panels) and (459872) 2014 EK₂₄ (brown empty circles in Fig. 3, left-hand side panels) are clear examples of Lidov–Kozai evolution, particularly in the case of Aten-class asteroid 2012 FC₇₁. The dynamical evolution of Apollo-class ($a > 1$ au and $q < 1.017$ au) asteroid 459872 is far more chaotic (the values of the various parameters change more rapidly and by a wider margin), but still displaying clear episodes of Lidov–Kozai resonant behaviour. In both cases, the value of the orbital inclination is low and the argument of perihelion tends to librate around 0° or 180°. The evolution of both objects has been studied in detail by de la Fuente Marcos & de la Fuente Marcos (2015b).

The evolution of Atira-class asteroid 2013 JX₂₈ (orange triangles in Fig. 3, right-hand side panels) and Aten-class asteroid 2016 XK₂₄ (green diamonds in Fig. 3, right-hand side panels) is somewhat similar to those presented in Fig. 2, although the inclinations are lower and the eccentricities higher. Asteroid 2016 XK₂₄ has the lowest value of the sidereal orbital period and 2013 JX₂₈ the third lowest. Aten-class asteroid 2016 XK₂₄ shows that the widespread dynamical behaviour found for the Atiras — i.e. coupled oscillation of the values of eccentricity and inclination, but no libration of the value of the argument of perihelion— is not exclusive of this dynamical class. Rather puzzling is the evolution of the recently discovered Aten-class asteroid 2019 BE₅ (Ohsawa et al. 2019),⁵ which exhibits libration of the argument of perihelion around -90° (or 270°) and has the fourth lowest value of the semimajor axis among known bound minor bodies, 0.61019 ± 0.00011 au (pink filled circles in Fig. 3, right-hand side panels), and a minimum orbit intersection distance, or MOID, with the Earth of 0.000163 au. The Lidov–Kozai resonant behaviour displayed by 2019 BE₅ is puzzling because it has a low value of the orbital inclination during the resonant episodes; the object follows a rather eccentric orbit and this fact may explain why ω does not librate around 0° or 180°. Its orbit determination is rather uncertain

⁵ <https://minorplanetcenter.net/mpec/K19/K19C10.html>

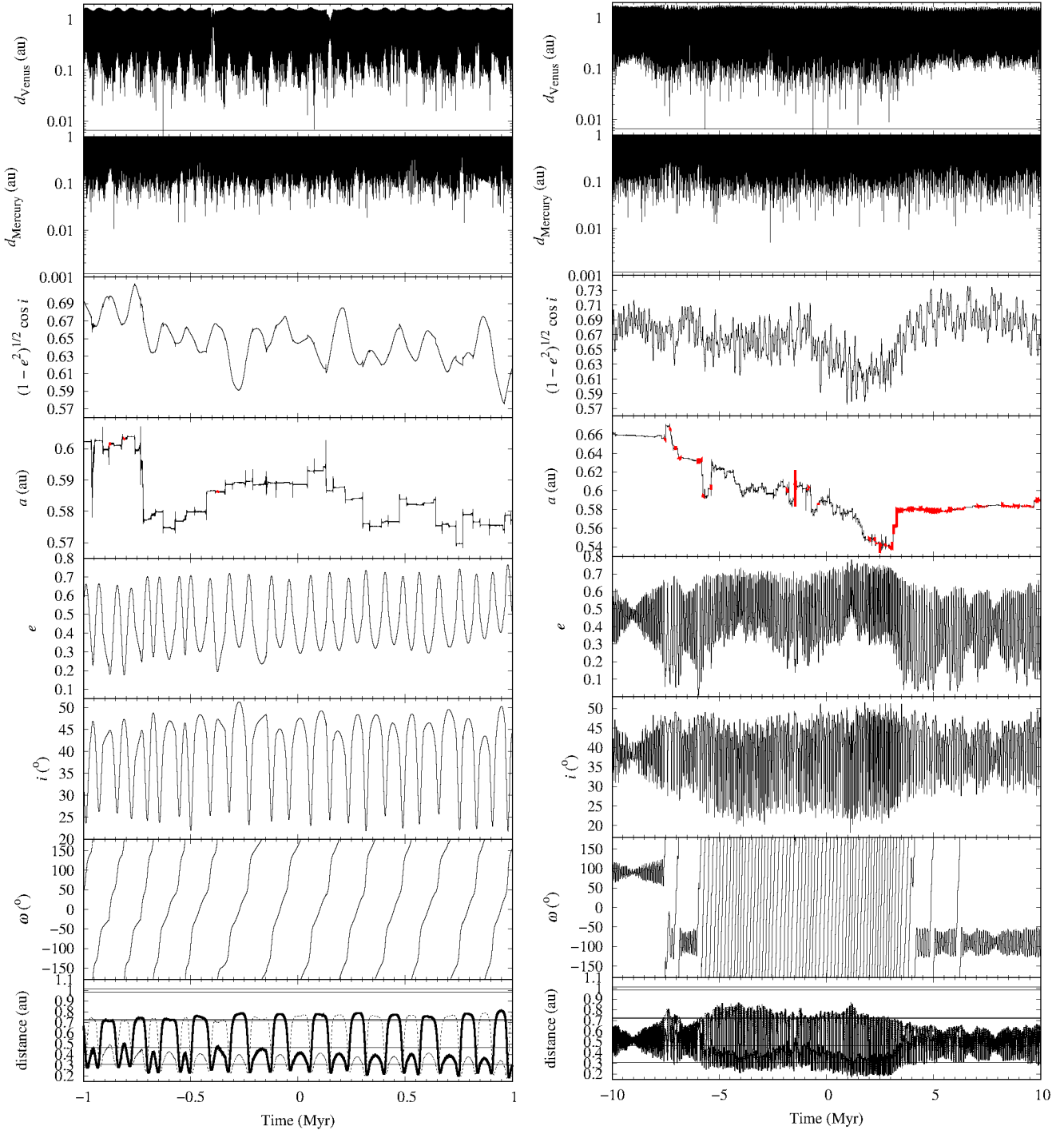


Figure 1. Evolution of the values of relevant parameters for the nominal orbit of 2019 AQ₃ (the left-hand side set of panels is a magnified version of the one on the right-hand side): distance from Venus (top panel, with Hill radius of Venus, 0.0067 au), distance from Mercury (second to top panel, with Hill radius of Mercury, 0.0012 au), value of the Lidov–Kozai parameter (third to top panel), semimajor axis (fourth to top panel, when the object becomes a Vatira it is plotted in thick red/grey), eccentricity (fourth to bottom panel), inclination (third to bottom panel), argument of perihelion (second to bottom panel), and nodal distances from the Sun (bottom panel, to descending node as thick line and to ascending node as dotted line, the aphelion and perihelion distances of Mercury, Venus, and the Earth are indicated as well).

though as it is based on 76 observations with a data-arc span of 8 d.

3.2 Short-term orbital evolution with respect to the invariable plane

So far, we have computed the orbital elements with respect to the ecliptic which is particular to the Earth and not significant for the

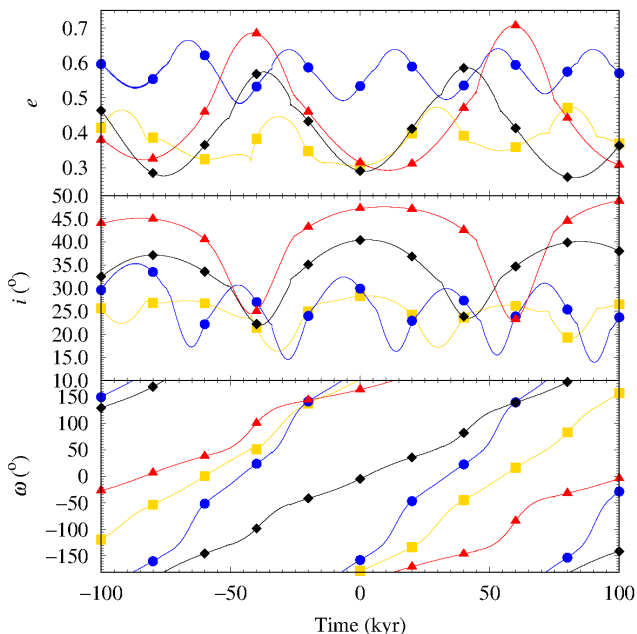


Figure 2. Evolution of the values of the eccentricity (top panel), inclination (middle panel), and argument of perihelion (bottom panel) of the nominal orbits of representative Atira-class asteroids: (418265) 2008 EA₃₂ (gold squares), 2010 XB₁₁ (blue circles), 2018 JB₃ (black diamonds), and 2019 AQ₃ (red triangles).

entire Solar system. A dynamically more relevant plane is in the invariable plane of the Solar system that is defined as the plane through the barycentre that is normal to the angular momentum vector of the Solar system, which is a constant of the motion. Souami & Souchay (2012) have shown that the ecliptic is within a few degrees of the invariable plane; the situation is equivalent to the one depicted in their fig. 1. The transformation between coordinates and velocities in the ecliptic frame of reference to the invariable plane is carried out by rotating first an angle Ω_{inv} about the z -axis and then an angle i_{inv} about the x -axis —rotation matrices in Souami & Souchay (2012) replacing φ with Ω_{inv} and ϵ with i_{inv} . The osculating values of Ω_{inv} and i_{inv} have been obtained using the equations (5) and (6) in Souami & Souchay (2012) that make use of equations (1) to (4) in section 2.2 of the same work. At output time, we have computed the instantaneous values of Ω_{inv} and i_{inv} using these equations, and changed the position and velocity vectors to the invariable plane before computing the orbital elements in the new frame of reference. At $t = 0$, $i_{\text{inv}} = 1^{\circ}57809813$ and $\Omega_{\text{inv}} = 107^{\circ}58872717$; the values obtained by Souami & Souchay (2012) are $i_{\text{inv}} = 1^{\circ}34'43''.3$ ($1^{\circ}57870312$) and $\Omega_{\text{inv}} = 107^{\circ}34'56''$ ($107^{\circ}58227198$) at the epoch J2000.0. Figure 4 shows the short-term accuracy of our determination of the orientation of the invariable plane; therefore, our calculations are accurate enough to obtain reliable conclusions regarding the present-day operation (or not) of the Lidov–Kozai resonance in the case of known Atiras. Figure 5 shows the evolution of the values of e , i , and ω in the invariable reference frame and no libration of ω is observed. This result confirms that there are no known Atiras currently trapped in a Lidov–Kozai resonance, but Figs 1 and 6 clearly show that this situation may change in the future.

3.3 Medium-term evolution

Figure 1, right-hand side set of panels, shows the medium-term evolution (from 10 Myr into the past to 10 Myr into the future) of the values of relevant parameters for the nominal orbit of 2019 AQ₃. Close encounters with both Venus and Mercury are systematically avoided after about 3.5 Myr into the future (but also prior to 8 Myr into the past) and the value of the Lidov–Kozai parameter changes within a smaller interval as well. On this extended time-scale, the value of the semimajor axis (fourth to top panel) changes by about 20 per cent (i.e. the overall behaviour is obviously chaotic), although after about 3.5 Myr it remains nearly constant. Now Mercury becomes the main direct perturber, but the Earth–Moon system and Jupiter remain as distant secular perturbers.

3.3.1 Lidov–Kozai evolution

After about 3.5 Myr into the future, the dynamical context changes significantly; now Mercury becomes the main direct perturber. Prior to this, a close encounter with Venus leads 2019 AQ₃ to a rather smooth path with nearly constant semimajor axis that is no longer within the Atira orbital realm but within the Vatira one (in thick red/grey, fourth to top panel). Now the coupled oscillation of the three orbital parameters, e , i , and ω , is observed. The value of the argument of perihelion mostly librates about 270° . In other words, the aphelion takes place when 2019 AQ₃ is the farthest from the ecliptic plane or aphelion always occurs away from the orbital plane of Venus. The Lidov–Kozai resonance is in effect, protecting 2019 AQ₃ from close encounters with Venus.

Figure 6 is analogous to Fig. 1 but shows the long-term evolution of two relevant control orbits based on the nominal solution but adding (+, right-hand set) or subtracting (–, left-hand set) three times the corresponding uncertainty from each orbital element (the six of them) in Table 1. These two examples of orbit evolution using initial conditions that are very different from those associated with the nominal orbit (yet still marginally compatible with the observations) are not meant to show how large the dispersion of the various parameters could be as they change over time, but to indicate that the onset of the Lidov–Kozai resonance is not only restricted to the nominal orbit or its immediate dynamical neighbourhood. Episodes of Lidov–Kozai resonance lasting for more than 1 Myr are observed in both cases.

Naoz (2016) has studied the Lidov–Kozai mechanism and how it can secularly excite the value of the eccentricity until collisions with inner or outer perturbers are possible. Although the orbital architecture driving the evolution of 2019 AQ₃ appears to contribute to enhance the stability of the orbits in the sense of keeping them within a well-defined section of the available orbital parameter space, Fig. 1 indicates that the eccentricity may eventually reach values that lead the aphelion closer to the Earth–Moon system, perhaps triggering an impact or an ejection from NEA parameter space. Conversely, a larger value of the eccentricity may lead to a shorter perihelion and an eventual collision with the Sun or an ejection from the Solar system or into its outskirts. In our case, the value of the aphelion distance, that oscillates between those of the semimajor axes of Venus and the Earth, can become as high as 1.02 au (see Fig. 6, right-hand panel), opening the door to eventual impacts on our planet if one of the nodes reaches aphelion (see also Ribeiro et al. 2016). Members of the Atira population can eventually become impactors as a result of the complex orbital evolution discussed here and in the event of an impact, they will most probably come from out of the Sun’s glare.

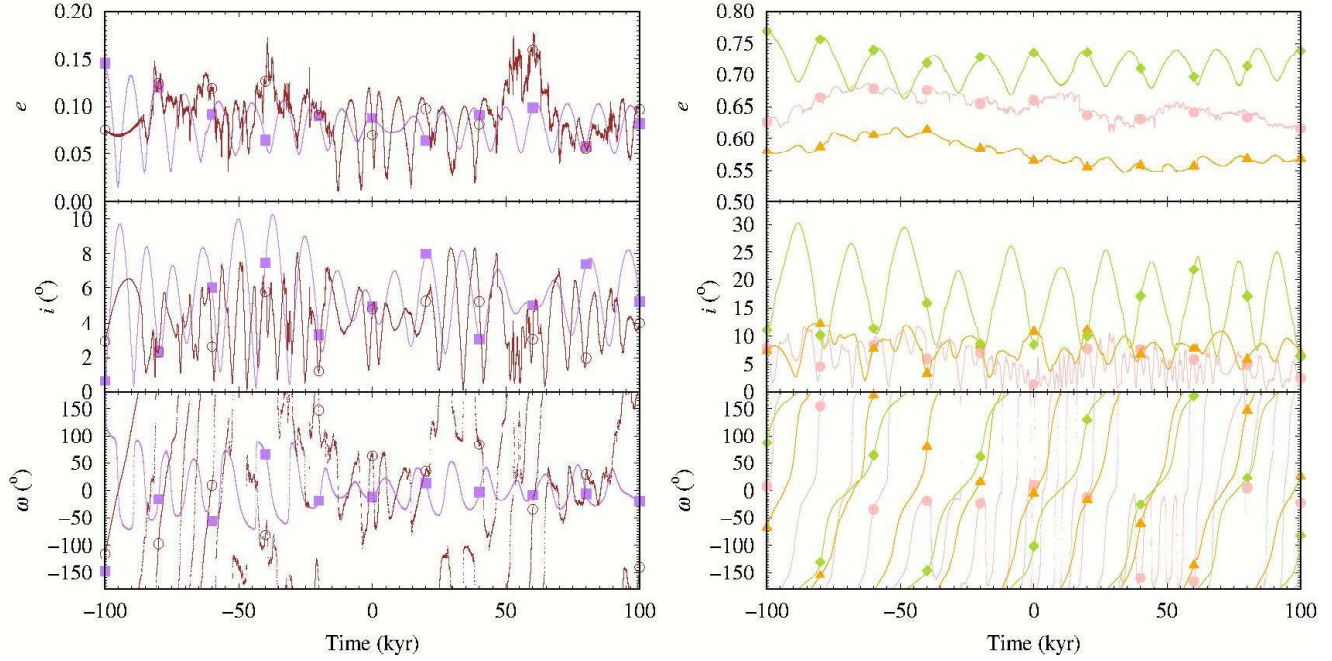


Figure 3. As Fig. 2 but for the nominal orbits of selected Atira, Aten, and Apollo asteroids: 2012 FC₇₁ (purple squares, Aten, left-hand side panels), 2013 JX₂₈ (orange triangles, Atira, right-hand side panels), (459872) 2014 EK₂₄ (brown empty circles, Apollo, left-hand side panels), 2016 XK₂₄ (green diamonds, Aten, right-hand side panels), and 2019 BE₅ (pink filled circles, Aten, right-hand side panels).

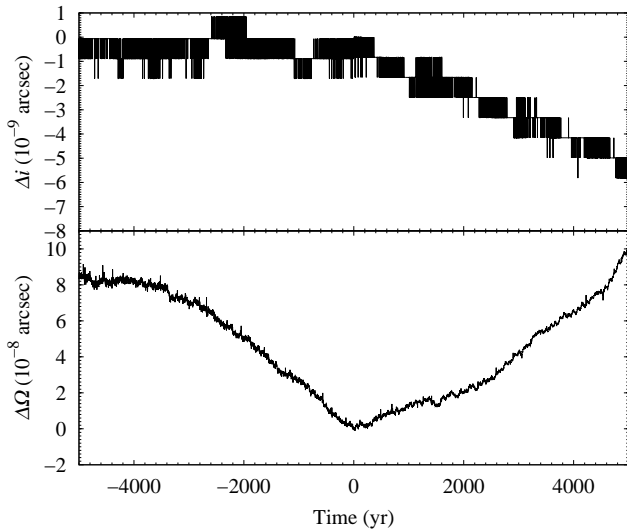


Figure 4. Temporal variations Δi (top panel) and $\Delta\Omega$ (bottom panel) in the orientation of the invariable plane of the system. $\Delta i = 0''$ ($\Delta\Omega = 0''$) corresponds to $i = 1^\circ.57809813$ ($\Omega = 107^\circ.58872717$) at $t = 0$.

3.3.2 *Vatira evolution*

The evolution of 2019 AQ₃ shown in Fig. 1 initially leads to brief periods (in thick red/grey) in which the aphelion distance of 2019 AQ₃, $Q < 0.718$ au i.e. 2019 AQ₃, an Atira, becomes a transient Vatira. This opens the door to transitions between the two dynamical classes. In fact, the dynamical context that keeps 2019 AQ₃ in a chaotic but relatively stable state may be effective in enabling a dynamical pathway to go from the Atira orbital realm into the Vatira one as shown by the evolution after about 3.5 Myr into the future. The progressive reduction in the value of the semimajor axis

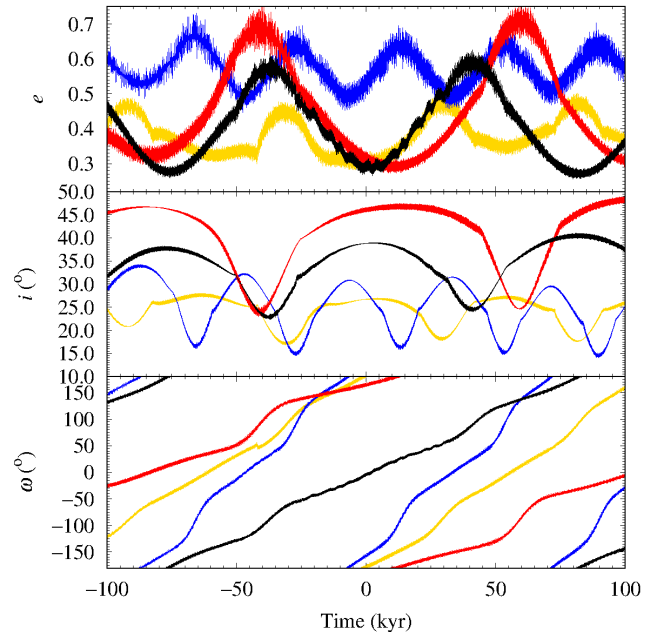


Figure 5. As Fig. 2 but with orbital elements computed in the frame of reference of the invariable plane of the system.

eventually leads to a transition from the Atira population into the Vatiras that avoid encounters with Venus altogether. Figure 6 shows that transitions to and from the Vatira orbital realm are also possible well away from the nominal orbit. Our calculations show that a combination of secular evolution and eventual close encounters with Venus triggers the transitions.

Atras do not cross the orbit of the Earth–Moon system and Vatiras do not cross the orbit of Venus; both Atras and Vatiras de-

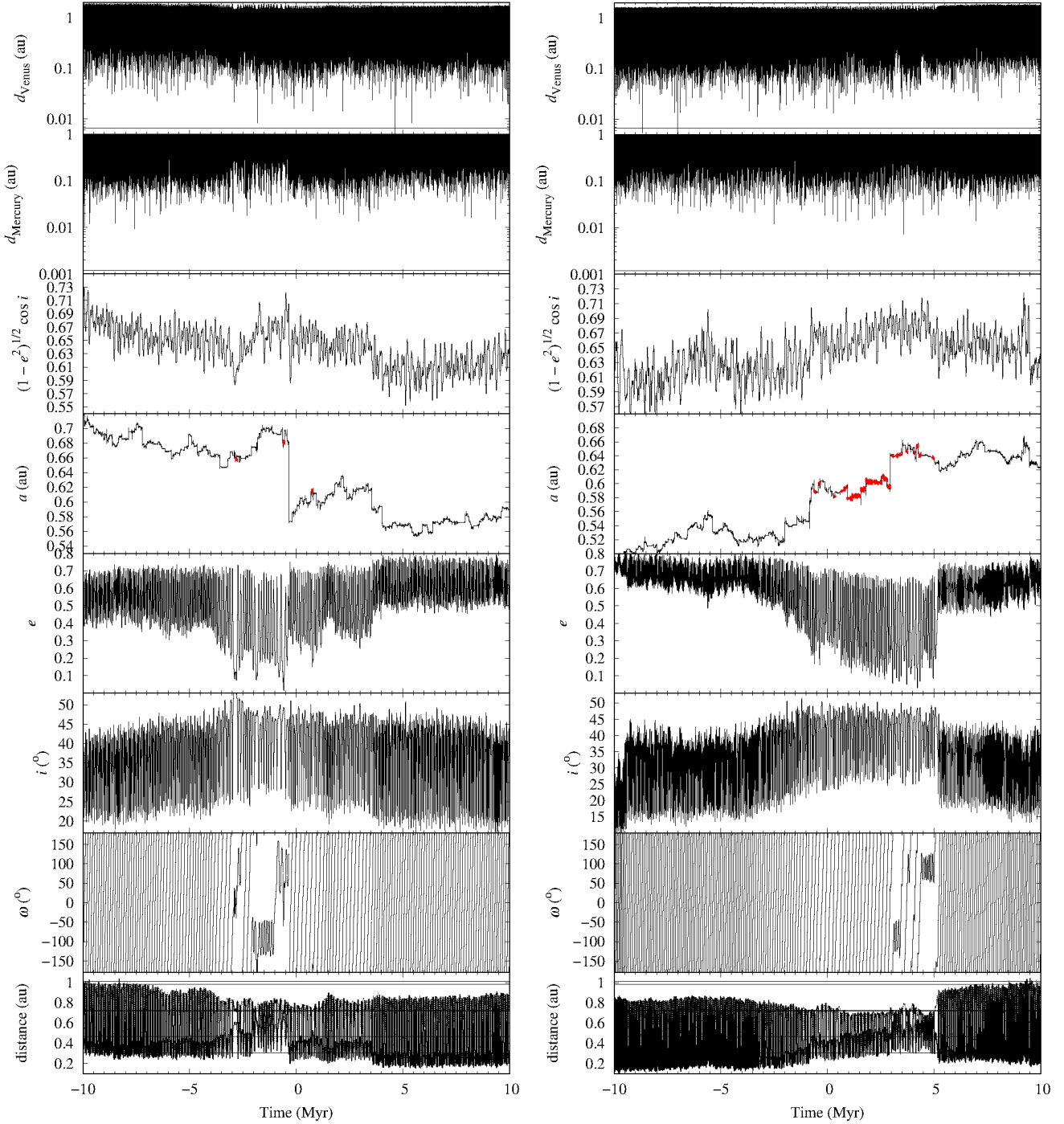


Figure 6. As Fig. 1 but for two control orbits that are most different from the nominal one (yet marginally compatible with the observations, see the text for details).

fine somewhat disjoint subsets. Atiras can impact on Venus, Vatiras cannot; therefore and although the members of both dynamical classes interact with Venus, they do it quite differently. We may now argue that the distinctive dynamical property of putative, long-term stable Vatiras is that they must be virtually and dynamically detached from Venus. This implies a robust difference between the dynamical behaviour of hypothetically stable Atiras, such as those discussed by Ribeiro et al. (2016), and stable Vatiras. In general, Atiras may still experience close encounters with Venus, Vatiras

cannot. When the Lidov–Kozai resonance is at work, in addition to avoiding close encounters with Venus at aphelion, close encounters with Mercury at perihelion are also reduced, but the orbit of Mercury is far more eccentric (0.21) and inclined (7°) than that of Venus. This aspect is more obvious when the evolution of the nodal distances is studied (bottom panels in Figs 1 and 6). After about 3.5 Myr into the future, the orbital nodes remain well away from the path of Venus, which must improve the overall orbital stability of 2019 AQ₃. We observe that this situation may have happened in

the past, but a close encounter with Venus nearly 5.5 Myr ago led to an extended period of time in which the nodes of 2019 AQ₃ crossed regularly the path of Venus; however, 2019 AQ₃ was not a Vatira at that time (see Fig. 1, right-hand side panels).

3.4 Dominant perturbers of the short-term dynamics

The textbook description of the Lidov–Kozai mechanism (see e.g. Murray & Dermott 1999) includes the coupled oscillation of the values of e and i , in such a way that when the eccentricity is at its highest, the inclination is at its lowest (and vice versa), and the argument of perihelion librates about 0° or 180° when the value of the inclination is low and about 90° or 270° when the inclination is high; this keeps the value of the Lidov–Kozai parameter (see above) nearly constant. However, for 2019 AQ₃, Fig. 1, left-hand side set of panels, suggests a more complicated present-day arrangement that is still able to produce the familiar oscillation in e and i , but not in ω .

In our case, 2019 AQ₃ might be controlled by two direct perturbers, Venus and the Earth–Moon system, and a distant one, Jupiter. In order to test which perturber is actually responsible for the observed orbital evolution, we have performed additional simulations without the various planets. Relevant results from these simulations are shown in Fig. 7. When Venus is removed, the orbital evolution of 2019 AQ₃ changes only slightly and becomes smooth (pink squares curve in Fig. 7) as the kinks disappear (compare pink squares and red triangles curves). We interpret this result as strong evidence in favour of Venus being a secondary actor in this case. However, when either the Earth–Moon system (green filled circles curve in Fig. 7) or Jupiter (brown diamonds curve in Fig. 7) are removed from the calculations, the impact on the orbital evolution of 2019 AQ₃ is such that we can consider the coupled oscillatory behaviour in e and i as effectively broken. When either Mercury (violet \times curve in Fig. 7) or Saturn (orange empty circles curve in Fig. 7) are removed from the calculations, no significant effects are seen (i.e. their contribution is weaker than that of Venus). Figure 8 shows the evolution when only the Sun, Venus, the Earth–Moon system, and Jupiter are included in the calculations. The simplified system of three perturbers reproduces the observed evolution better than other arrangements and therefore we consider our interpretation as confirmed: the observed dynamical evolution is the result of the combined action of two dominant perturbers, the Earth–Moon system and Jupiter, and a secondary one, Venus.

3.5 Post-Newtonian evolution

Because of the effect of the secular dynamics discussed above, the perihelion distance of 2019 AQ₃ is always in the neighbourhood or inside the orbit of Mercury and can become as low as 0.17 au, below that of asteroids such as 1566 Icarus (1949 MA) for which relativistic motion in the form of non-Newtonian perihelion precession has been measured (see e.g. Sitarski 1992). However, the overall results of our calculations under the post-Newtonian approximation are consistent with those obtained in the Newtonian case (see Fig. 9). The post-Newtonian evolution (in grey) preserves the coupled oscillations in e and i observed under the Newtonian approximation (in black). The issue of general relativistic precession operating together with Lidov–Kozai oscillations has been explored by Sekhar et al. (2017). Although 2019 AQ₃ is not currently trapped in a Lidov–Kozai resonance, the overall evolution is preserved in the post-Newtonian case.

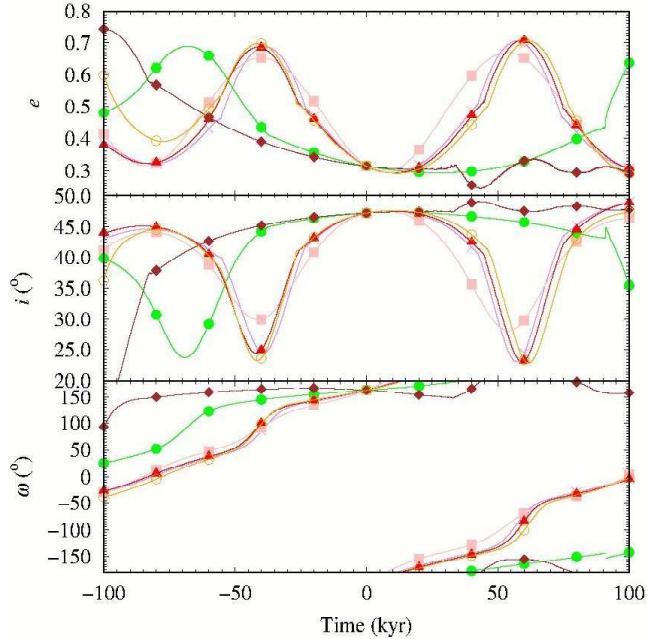


Figure 7. Evolution of the values of the eccentricity (top panel), inclination (middle panel), and argument of perihelion (bottom panel) of the nominal orbit of 2019 AQ₃ under the usual physical model (red triangles), without Mercury (violet \times), without Venus (pink squares), without the Earth–Moon system (green filled circles), without Jupiter (brown diamonds), and without Saturn (orange empty circles).

4 DISCUSSION

The data in Section 2.1 hint at a possible outlier nature of 2019 AQ₃ both within the known NEAs and even among the known Atiras. Table 2 shows the available orbital data for NEAs currently classified as members of the Atira dynamical class. On the one hand and considering the statistical parameters Q_3 , third quartile, IQR, interquartile range, and OU, upper outlier limit ($Q_3 + 1.5$ IQR, Tukey 1977), for the orbital inclination of the 19 known Atiras we obtain: $Q_3=26^\circ.94$, $IQR=13^\circ.36$, and $OU=46^\circ.99$. With a value of the inclination of $47^\circ.2186 \pm 0^\circ.0009$, 2019 AQ₃ barely qualifies as an outlier; however, it certainly is a strong outlier in terms of aphelion distance (0.773684 au versus $OL=0.825768$ au) — (418265) 2008 EA₃₂ is another outlier in Q (0.803780 au). On the other hand, a statistical analysis analogous to the one presented by de la Fuente Marcos & de la Fuente Marcos (2019) that used the orbit model⁶ developed by the Near-Earth Object Population Observation Program (NEOPOP) and described by Granvik et al. (2018) shows that 2019 AQ₃ is indeed a statistical outlier within the known NEA population. Because of its high orbital inclination, there are no other known objects with similar orbit determinations. The orbit model predicts the existence of five objects (for the entire NEO population with $H < 25$ mag, about 800 000 predicted NEOs) orbitally similar to 2019 AQ₃ but with absolute magnitudes, H , in the range 23–25 mag, considerably smaller than 2019 AQ₃. Therefore, it is an outlier within the known NEO orbits (perhaps due to observational bias, see e.g. Ribeiro et al. 2016), but also an outlier (in terms of size) when considering the predictions from a state-of-the-art orbit model. Regarding the overall size distribution of the known Atiras, there is an unusually large number of objects with

⁶ <http://neo.ssa.esa.int/neo-population>

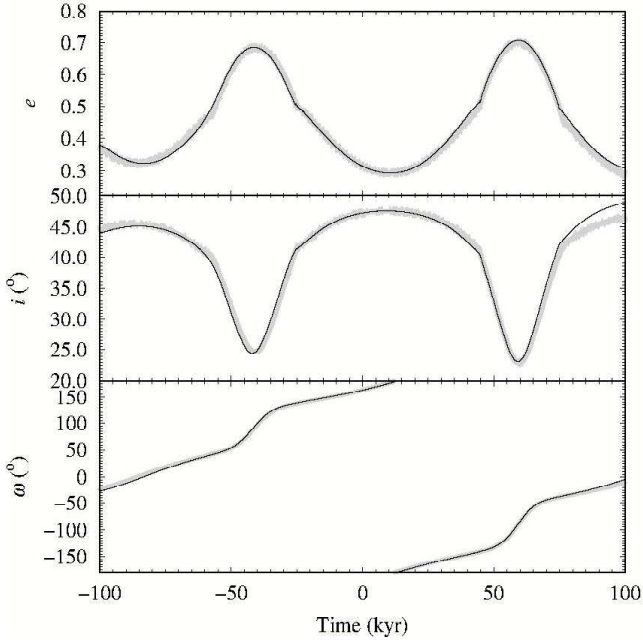


Figure 8. As Fig. 7, nominal orbit of 2019 AQ₃ under the usual physical model (solid black) and only with Venus, the Earth–Moon system, and Jupiter (thick solid light grey).

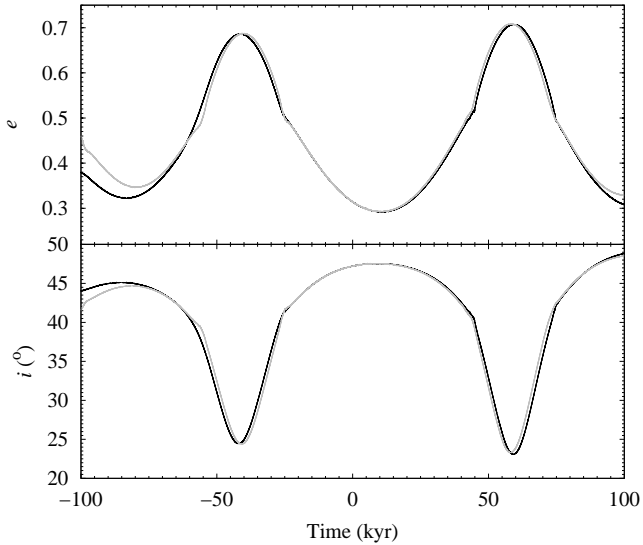


Figure 9. Evolution of the values of the eccentricity (top panel) and inclination (bottom panel) of the nominal orbit of 2019 AQ₃ under the Newtonian (in black) and post-Newtonian (in grey) approximations.

$H < 23\text{--}25$ mag (see last column in Table 2). Figure 10 shows the evolution of 2018 JB₃ that goes from Aten to Atira and eventually becomes a Vatira. This dynamical evolution suggests that the Atira/Vatira orbital realm may be repopulated with former Atens.

Our results are robust, a representative set of control orbits (500) using the covariance matrix approach (see Section 2.2) give consistent results within a few thousand years of our reference epoch. Dispersions resemble those in fig. 3 of de la Fuente Marcos & de la Fuente Marcos (2019). It is however worth to mention that close encounters with Venus (see Fig. 1, top panel, left-hand side set), may induce significant orbital changes

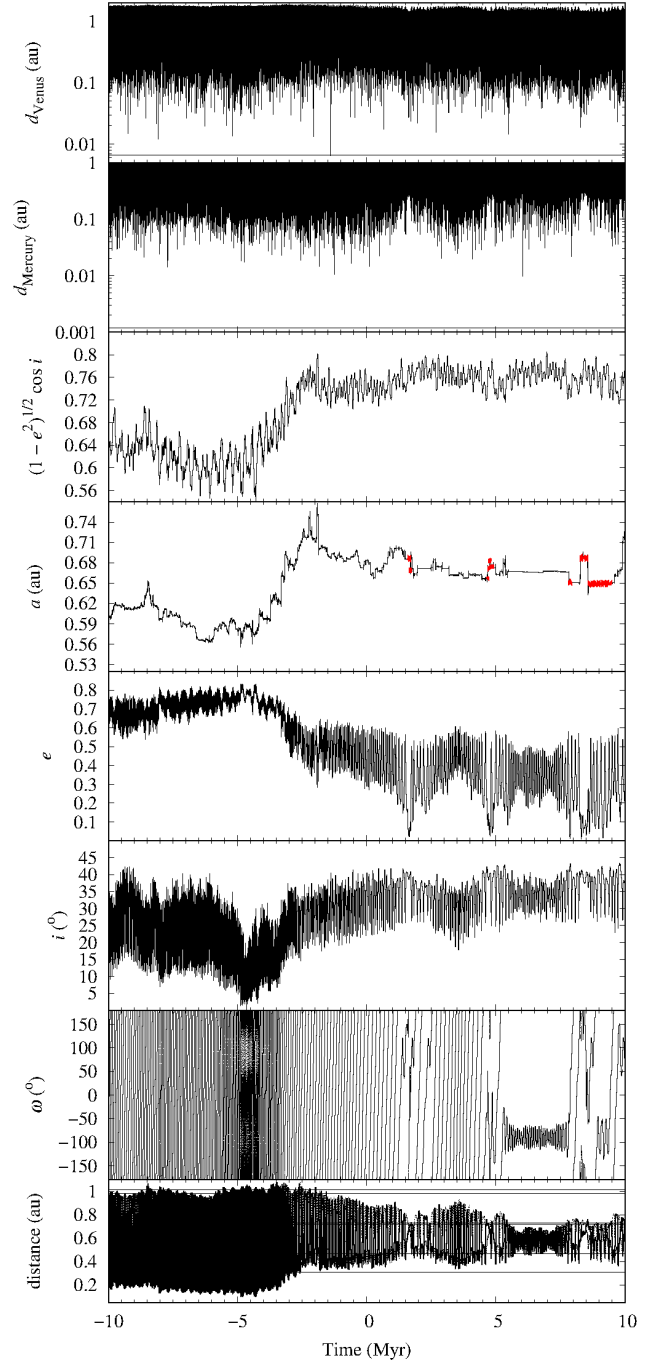


Figure 10. As Fig. 1 but for the nominal orbit of 2018 JB₃.

although the resulting orbit still remains within the Atira orbital realm.

Atiras have an intrinsic interest within the context of planetary defense (see e.g. Mainzer 2017) as they are major candidates to experience the so-called Red Baron dynamical scenario (Adamo 2011) in which an asteroid approaches our planet from out of the Sun’s glare. A recent example of Red Baron scenario event that resulted in an impact is the one associated with the Chelyabinsk superbolide (de la Fuente Marcos & de la Fuente Marcos 2013b; Popova et al. 2013), although in this case the parent body was not a member of the Atira class.

Table 2. Heliocentric orbital elements and parameters — $q = a(1 - e)$ is the perihelion distance, $Q = a(1 + e)$ is the aphelion distance— of the known Atiras. The statistical parameters are Q_1 , first quartile, Q_3 , third quartile, IQR, interquartile range, OL, lower outlier limit ($Q_1 - 1.5$ IQR), and OU, upper outlier limit ($Q_3 + 1.5$ IQR). The orbit determinations are referred to epoch JD 2458600.5 (2019-Apr-27.0) TDB (J2000.0 ecliptic and equinox) with the exception of 1998 DK₃₆ (JD 2450868.5 TDB) and 2015 ME₁₃₁ (JD 2457197.5 TDB). Source: JPL’s SBDB.

Object	a (au)	e	i (°)	Ω (°)	ω (°)	q (au)	Q (au)	H (mag)
(163693) Atira	0.740919	0.322122	25.620193	103.888396	252.886331	0.502253	0.979585	16.3
(164294) 2004 XZ ₁₃₀	0.617615	0.454551	2.950756	211.373871	5.180663	0.336878	0.898353	20.4
(413563) 2005 TG ₄₅	0.681393	0.372181	23.336466	273.436802	230.416868	0.427792	0.934994	17.6
(418265) 2008 EA ₃₂	0.615907	0.305035	28.264395	100.958641	181.840605	0.428034	0.803780	16.4
(434326) 2004 JG ₆	0.635232	0.531142	18.943867	37.029381	352.998487	0.297834	0.972631	18.4
(481817) 2008 UL ₉₀	0.695049	0.379850	24.309761	81.142712	183.642522	0.431034	0.959063	18.6
1998 DK ₃₆	0.692257	0.416017	2.017520	151.461720	180.042707	0.404267	0.980248	25.0
2006 WE ₄	0.784745	0.182918	24.767078	311.014633	318.597466	0.641201	0.928288	18.9
2010 XB ₁₁	0.618029	0.533873	29.886574	96.315122	202.484306	0.288080	0.947978	19.9
2012 VE ₄₆	0.713043	0.361305	6.675782	8.784572	190.539803	0.455417	0.970669	20.2
2013 JX ₂₈	0.600855	0.564131	10.761830	39.955081	354.887304	0.261894	0.939815	20.1
2013 TQ ₅	0.773707	0.155579	16.398688	286.770884	247.296796	0.653334	0.894079	19.8
2014 FO ₄₇	0.752123	0.271100	19.197106	358.653061	347.463144	0.548222	0.956023	20.3
2015 DR ₂₁₅	0.666400	0.471499	4.088461	314.953867	42.283540	0.352193	0.980607	20.3
2015 ME ₁₃₁	0.806118	0.204225	30.236744	315.351877	162.273931	0.641489	0.970747	19.5
2017 XA ₁	0.809618	0.201567	17.176997	239.659585	327.622064	0.646426	0.972811	21.2
2017 YH	0.634446	0.482474	19.833554	134.222643	147.454605	0.328342	0.940550	18.5
2018 JB ₃	0.683189	0.290494	40.392589	106.425908	355.237492	0.484726	0.881651	17.6
2019 AQ ₃	0.588662	0.314310	47.218559	64.487327	163.151818	0.403639	0.773684	17.6
Mean	0.689963	0.358651	20.635627	170.309794	223.489497	0.449108	0.930819	19.29
Standard deviation	0.071367	0.125388	12.148875	112.633878	102.342995	0.127856	0.058487	1.97
Median	0.683189	0.361305	19.833554	134.222643	202.484306	0.428034	0.947978	19.50
Q_1	0.626238	0.280797	13.580259	88.728917	171.597263	0.344535	0.913321	18.00
Q_3	0.746521	0.463025	26.942293	280.103843	323.109765	0.525238	0.971689	20.25
IQR	0.120283	0.182228	13.362034	191.374926	151.512502	0.180702	0.058368	2.25
OL	0.445813	0.007455	-6.462792	-198.333472	-55.671490	0.073482	0.825768	14.63
OU	0.926946	0.736367	46.985344	567.166232	550.378518	0.796291	1.059242	23.63

Regarding the discoverability of these objects, *Gaia* (Gaia Collaboration, Prusti et al. 2016) may observe a number of objects at relatively low solar elongations (see fig. 10 in Gaia Collaboration, Spoto et al. 2018) and also scan at extreme inclinations with respect to the ecliptic. Large Atiras and even Vatiras (apparent visual magnitude < 19) at high inclination may be within reach of *Gaia*. Vatiras may reach their aphelia more than twice per year, which increases the probability of accidental detection of such objects.

5 CONCLUSIONS

In this paper, we have explored the orbital evolution of 2019 AQ₃, which has the shortest aphelion of any known minor body, using direct N -body simulations under the Newtonian and post-Newtonian approximations. Our conclusions are as follows:

- (i) The present-day orbital evolution of 2019 AQ₃ is relatively smooth as a result of being affected by the combined action of the Earth–Moon system and Jupiter with Venus as a secondary perturber. The Lidov–Kozai mechanism is not at work here as the argument of perihelion of 2019 AQ₃ does not librate, but circulates. This property is shared by several of the known Atira-class asteroids and by some Atens.
- (ii) Our calculations indicate that 2019 AQ₃ may have experi-

enced brief stints as a Vatira in the relatively recent past and it may become a full-time Vatira in the near future after undergoing a close encounter with Venus, outlining a viable dynamical pathway that may transform Atiras into Vatiras. Our calculations show that stable Vatiras can be trapped in a Lidov–Kozai resonance that protects them from close encounters with Venus.

- (iii) Atira-class asteroid 2019 AQ₃ is an outlier within the known NEO orbits, but also an outlier (in terms of size) when considering the predictions from a state-of-the-art orbit model. Among the known Atiras, it is a clear outlier in terms of aphelion distance.
- (iv) The orbital evolution discussed here may keep Atiras switching between relatively close trajectories for extended periods of time, but also transform Atiras into eventual Earth impactors coming from out of the Sun’s glare.
- (v) Although the value of the perihelion distance of 2019 AQ₃ can become as low as 0.17 au, the inclusion of post-Newtonian terms in the numerical integrations does not significantly affect the overall orbital evolution.
- (vi) The dynamical evolution of the Atira-class asteroid 2018 JB₃ shows that Atens may evolve into Atiras/Vatiras and therefore repopulate these dynamical classes when members are lost.

Atira-class asteroid 2019 AQ₃ is indeed a statistical outlier within

the context of known NEAs, but it is also a rare and important discovery that heralds a new dynamical class, that made of those NEAs following orbits entirely encompassed within that of Venus: the Vatiras originally proposed by Greenstreet et al. (2012). The evolution of the solar elongation of 2019 AQ₃ is similar to that of Venus with maximum elongation at about 47°. When observing from the ground, finding true Vatiras requires the observation at elongations below 45°. This is at the edge of the minimum solar elongation scanned by the spacecraft *Gaia* and it cannot be discarded that a true Vatira will be observed during the mission. A systematic exploration of the Vatira orbital realm requires a well-designed, space-based mission.

ACKNOWLEDGEMENTS

We thank the referee for his/her constructive reports and very helpful suggestions regarding the presentation of this paper and the interpretation of our results, S. J. Aarseth for providing the code used in this research, O. Vaduvescu, F. Roig, M. N. De Prá, and S. Deen for comments, and A. I. Gómez de Castro for providing access to computing facilities. This work was partially supported by the Spanish ‘Ministerio de Economía y Competitividad’ (MINECO) under grants ESP2015-68908-R and ESP2017-87813-R. In preparation of this paper, we made use of the NASA Astrophysics Data System and the Minor Planet Center data server.

REFERENCES

- Aarseth S. J., 2003, Gravitational N-body Simulations. Cambridge Univ. Press, Cambridge, p. 27
- Adamo D. R., 2011, Horizons Newsl., June 2011, p. 64
- Bellm E., Kulkarni S., 2017, Nat. Astron., 1, 0071
- Benitez F., Gallardo T., 2008, Celest. Mech. Dyn. Astron., 101, 289
- Buzzi L. et al., 2019, MPEC Circ., MPEC 2019-A88
- Chambers K. et al., 2019, MPEC Circ., MPEC 2019-A97
- de la Fuente Marcos C., de la Fuente Marcos R., 2012, MNRAS, 427, 728
- de la Fuente Marcos C., de la Fuente Marcos R., 2013a, MNRAS, 432, 886
- de la Fuente Marcos C., de la Fuente Marcos R., 2013b, MNRAS, 436, L15
- de la Fuente Marcos C., de la Fuente Marcos R., 2014, MNRAS, 439, 2970
- de la Fuente Marcos C., de la Fuente Marcos R., 2015a, MNRAS, 453, 1288
- de la Fuente Marcos C., de la Fuente Marcos R., 2015b, A&A, 580, A109
- de la Fuente Marcos C., de la Fuente Marcos R., 2018, Res. Notes AAS, 2, 46
- de la Fuente Marcos C., de la Fuente Marcos R., 2019, MNRAS, 483, L37
- de la Fuente Marcos C., de la Fuente Marcos R., Aarseth S. J., 2015, MNRAS, 446, 1867
- Durda D. D., Stern S. A., Colwell W. B., Parker J. W., Levison H. F., Hassler D. M., 2000, Icarus, 148, 312
- Evans N. W., Tabachnik S., 1999, Nature, 399, 41
- Evans N. W., Tabachnik S. A., 2002, MNRAS, 333, L1
- Farinella P., Froeschle Ch., Froeschle C., Gonczi R., Hahn G., Morbidelli A., Valsecchi G. B., 1994, Nature, 371, 315
- Gaia Collaboration, Prusti T. et al., 2016, A&A, 595, A1
- Gaia Collaboration, Spoto, F. et al., 2018, A&A, 616, A13
- Giorgini J., 2011, in Capitaine N., ed., Proceedings of the Journées 2010 “Systèmes de référence spatio-temporels” (JSR2010): New challenges for reference systems and numerical standards in astronomy, Observatoire de Paris, Paris, p. 87
- Giorgini J. D., 2015, IAU General Assembly, Meeting #29, 22, 2256293
- Giorgini J. D., Yeomans D. K., 1999, On-Line System Provides Accurate Ephemeris and Related Data, NASA TECH BRIEFS, NPO-20416, p. 48
- Giorgini J. D. et al., 1996, BAAS, 28, 1158
- Giorgini J. D., Chodas P. W., Yeomans D. K., 2001, BAAS, 33, 1562
- Granvik M. et al., 2018, Icarus, 312, 181
- Greenstreet S., Ngo H., Gladman B., 2010, AAS/Div. Planet. Sci. Meeting Abstr., 42, 13.09
- Greenstreet S., Ngo H., Gladman B., 2012, Icarus, 217, 355
- Hernandez D. M., Bertschinger E., 2015, MNRAS, 452, 1934
- Hernandez D. M., Bertschinger E., 2018, MNRAS, 475, 5570
- Kaiser N., 2004, SPIE, 5489, 11
- Kaiser N., Pan-STARRS Project Team, 2004, BAAS, 36, 828
- Kozai Y., 1962, AJ, 67, 591
- Laskar J., Fienga A., Gastineau M., Manche H., 2011, A&A, 532, A89
- Libert A.-S., Tsiganis K., 2009, A&A, 493, 677
- Lidov M. L., 1962, Planet. Space Sci., 9, 719
- Mainzer A., 2017, JGRE, 122, 789
- Makino J., 1991, ApJ, 369, 200
- Masi G., 2003, Icarus, 163, 389
- Michel P., Thomas F., 1996, A&A, 307, 310
- Michel P., Zappalà V., Cellino A., Tanga P., 2000, Icarus, 143, 421
- Milani A., Nobili A. M., 1992, Nature, 357, 569
- Milani A., Carpino M., Hahn G., Nobili A. M., 1989, Icarus, 78, 212
- Murray C. D., Dermott S. F., 1999, Solar System Dynamics, Cambridge Univ. Press, Cambridge, p. 316
- Naoz S., 2016, ARA&A, 54, 441
- Ohsawa R. et al., 2019, MPEC Circ., MPEC 2019-C10
- Popova O. P. et al., 2013, Science, 342, 1069
- Ribeiro A. O., Roig F., De Prá M. N., Carvano J. M., DeSouza S. R., 2016, MNRAS, 458, 4471
- Rivera-Valentin E. G., Taylor P. A., Virkki A., Aponte-Hernandez B., 2017, CBET, 4347
- Schumacher G., Gay J., 2001, A&A, 368, 1108
- Sekhar A., Asher D. J., Werner S. C., Vaubaillon J., Li G., 2017, MNRAS, 468, 1405
- Sitarski G., 1992, AJ, 104, 1226
- Smith R. M. et al., 2014, SPIE, 9147, 914779
- Souami D., Souchay J., 2012, A&A, 543, A133
- Standish E. M., 1998, JPL Planetary and Lunar Ephemerides, DE405/LE405, Interoffice Memo. 312.F-98-048, Jet Propulsion Laboratory, Pasadena, California
- Steffl A. J., Cunningham N. J., Shinn A. B., Durda D. D., Stern S. A., 2013, Icarus, 223, 48
- Stern S. A., Durda D. D., 2000, Icarus, 143, 360
- Tholen D. J., 1998, MPBu, 25, 42
- Tholen D. J., Whiteley R. J., 1998, AAS/Div. Planet. Sci. Meeting Abstr., 30, 16.04
- Tukey J. W., 1977, Exploratory Data Analysis. Addison-Wesley, Reading, MA
- Varadi F., Runnegar B., Ghil M., 2003, ApJ, 592, 620
- Vokrouhlický D., Farinella P., Bottke W. F., 2000, Icarus, 148, 147
- Wall J. V., Jenkins C. R., 2012, Practical Statistics for Astronomers. Cambridge Univ. Press, Cambridge
- Warell J., Karlsson O., Skoglöv E., 2003, A&A, 411, 291
- Whiteley R. J., Tholen D. J., 1998, AAS/Div. Planet. Sci. Meeting Abstr., 30, 16.03
- Zavodny M., Jedicke R., Beshore E. C., Bernardi F., Larson S., 2008, Icarus, 198, 284

This paper has been typeset from a $\text{\TeX}/\text{\LaTeX}$ file prepared by the author.